

# Lawrence Berkeley National Laboratory

## Recent Work

### Title

ANNEALING OF FAULTED LOOPS IN GOLD

### Permalink

<https://escholarship.org/uc/item/9ds7c6j1>

### Author

Brun, Georges.

### Publication Date

1966-09-01

UCRL-17060

**University of California**  
**Ernest O. Lawrence**  
**Radiation Laboratory**

ANNEALING OF FAULTED LOOPS IN GOLD

**TWO-WEEK LOAN COPY**

*This is a Library Circulating Copy  
which may be borrowed for two weeks.  
For a personal retention copy, call  
Tech. Info. Division, Ext. 5545*

**Berkeley, California**

## **DISCLAIMER**

This document was prepared as an account of work sponsored by the United States Government. While this document is believed to contain correct information, neither the United States Government nor any agency thereof, nor the Regents of the University of California, nor any of their employees, makes any warranty, express or implied, or assumes any legal responsibility for the accuracy, completeness, or usefulness of any information, apparatus, product, or process disclosed, or represents that its use would not infringe privately owned rights. Reference herein to any specific commercial product, process, or service by its trade name, trademark, manufacturer, or otherwise, does not necessarily constitute or imply its endorsement, recommendation, or favoring by the United States Government or any agency thereof, or the Regents of the University of California. The views and opinions of authors expressed herein do not necessarily state or reflect those of the United States Government or any agency thereof or the Regents of the University of California.

UCRL-17060

UNIVERSITY OF CALIFORNIA  
Lawrence Radiation Laboratory  
Berkeley, California  
AEC Contract No. W-7405-eng-48

ANNEALING OF FAULTED LOOPS IN GOLD

Georges Brun

(M.S. Thesis)

September 1966

TABLE OF CONTENTS

Abstract

I. Introduction . . . . . 1

    A. Tetrahedral Stacking Faults . . . . . 1

    B. Faulted Loops . . . . . 2

    C. Perfect Loops . . . . . 2

    D. Black Spot Defects . . . . . 2

II. Experimental Procedure . . . . . 3

    A. Heat Treatment . . . . . 3

    B. Electropolishing . . . . . 4

    C. The Microscope . . . . . 4

III. Results . . . . . 6

    A. Faulted Loops in Gold . . . . . 6

    B. Shrinkage of Defects . . . . . 9

IV. Discussion . . . . . 10

    A. Formation of Faulted Loops . . . . . 10

    B. Shrinkage of Loops . . . . . 11

V. Conclusions . . . . . 14

Acknowledgments . . . . . 15

Tables . . . . . 16

References . . . . . 18

Figure Captions . . . . . 20

Figures . . . . . 22

ANNEALING OF FAULTED LOOPS IN GOLD

Georges Brun

Inorganic Materials Research Division, Lawrence Radiation Laboratory,  
Department of Mineral Technology, College of Engineering,  
University of California, Berkeley, California

ABSTRACT

Faulted loops rather than stacking fault tetrahedra are found in quenched gold if the aging temperature is raised to 150°C.

The shape of these loops is discussed and both theoretical calculations and observation under the electron microscope show that they are extended.

Hot stage experiments show that the shrinkage occurs at 340°C, the loops always keeping a prismatic shape. This is explained in terms of a ledge mechanism.

## I. INTRODUCTION

Large vacancy supersaturation can be obtained in gold by quenching from near the melting point to room temperature; during a subsequent annealing, the vacancies collapse into clusters to reduce the free energy of the crystal. Four different categories of clusters were found.

### A. Tetrahedral Stacking Faults

Tetrahedra of stacking fault were first observed by Silcox and Hirsch.<sup>1</sup> These defects consist of four stacking faults in four different (111) planes, joined by stair rod dislocations. Their sizes varied from 100Å to 4,000Å. Their images depended on the orientation of the foil and the diffracting conditions (Fig. 1).

The formation mechanism of tetrahedra has been considered by several authors:

#### 1. Vacancy Clustering and Dislocation Glide (Silcox and Hirsch<sup>1</sup>)

The first step was considered to be a Frank triangle formed by collapse of vacancy discs. The  $1/3$  [111] dislocation can split into a stair rod and a Shockley on each of the intersecting (111) planes; these Shockleys can glide in their glide planes to form a tetrahedron.

#### 2. Dislocation Glide (Hirsch<sup>2</sup> and Loretto<sup>3</sup>)

In this case the triangular Frank loop could be formed by cross slip of an extended dislocation at a jog. Then the same glide process as above is involved to form a tetrahedron.

#### 3. Direct Vacancy Clustering (De Jong and Koehler,<sup>4</sup> Kimura et al.,<sup>5</sup> Cotterill and Doyama,<sup>6</sup> Kuhlmann Wilsdorff et al.,<sup>7,8</sup> Czjzek et al.<sup>9</sup>)

A tetravacancy may act as a nucleus which grows into a tetrahedron by absorption of vacancies at the edges.

### B. Faulted Loops (Fig. 5)

Faulted loops were first observed also by Silcox and Hirsch<sup>1</sup> and their presence explained as the product of destruction of the tetrahedra. They always lay in (111) planes and their sides were always along the [110] directions. Their sizes varied from about 200Å to 4,000Å. A discussion about their real shape is given later.

### C. Perfect Loops (Fig. 2, Detail G)

A few perfect prismatic loops were found. They were supposed to have been formed by nucleation of a Shockley at the center of a faulted loop. This mechanism has been discussed by Saada.<sup>10</sup> He found that this was possible only under a high stress. It is likely that these loops are formed during the observation in the microscope, due to local heating of the specimen by the electron beam.

### D. Black Spot Defects

When gold was quenched from a low temperature (under 800°C), and then aged at 100°C, few tetrahedra were formed, instead black spot defects appeared. Their nature has been discussed by Meshii,<sup>11</sup> and Cotterill.<sup>12,13</sup> The use of dark field strain contrast techniques would solve this problem.<sup>28</sup>

Most of the work performed on gold has been concerned with the mechanisms of the formation, growth or annealing of tetrahedra.

For obvious reasons, formation of tetrahedra is impossible to observe directly under the electron microscope.

First Silcox,<sup>26</sup> then Segall et al.<sup>27</sup> attempted to observe annealing of tetrahedra in hot stage experiments. No useful results were obtained

because surface diffusion or evaporation eliminates the thinnest regions of the foil at a temperature below that at which tetrahedra shrink.

Therefore no experimental evidence of these mechanisms has yet been given. For reasons exposed later, it is believed that faulted loops shrink with the same mechanism as tetrahedra, but at a lower temperature. Therefore the shrinkage can be observed in hot stage experiments. This is the object of the present work.

## II. EXPERIMENTAL PROCEDURE

The material used was 99.999% gold, the main impurity being Ag:3 ppm. The specimens were 2 X 1 in. and 3 mil thick. This was small enough to avoid too much strain during the quench, but large enough to get several electron microscope specimens by electropolishing.

### A. Heat Treatment

Specimens were first held at 1000°C for two days in air. This allowed the grains to grow and the dislocation density to be reduced. It was also found that this treatment reduced the concentration of impurities.<sup>14</sup>

The specimen was heated for 20 minutes to 1050°C±5°C and then quenched to a selected temperature between +80°C and -20°C in a brine solution. Quenching curves were recorded on an oscillograph with a triggering system (Fig. 4).

Immediately after the quench the specimens were put in a furnace for an aging treatment. The time elapsed between quenching and introduction into the furnace was made as short as possible, usually about 20 seconds. During this time preaging takes place as emphasized by Meshii.<sup>11</sup>

The aging temperatures were varied from 100°C to 400°C for periods between 1/2 hour to 48 hours. Though the resulting defect substructure was not very reproducible, it was consistent with the previous observations by Meshii.<sup>11</sup>

At 1050°C the equilibrium concentration of vacancies in gold is of the order of  $10^{-4}$ . By rapid quench into a bath at 70°C or below, a significant fraction was retained, resulting in growth of large numbers of vacancy defects during aging.

Quenching curves for a bath temperature of 20°C are shown in Fig. 4a,b. The initial cooling rate was about 20,000°C/sec.

Large vacancy defects were obtained by keeping the preaging time as short as possible so that only a few nuclei were formed. The effect of increasing preaging time from 20 seconds to 2 minutes is illustrated by Figs. 2 and 3. The longer preaging time results in nucleation of many more defects. After aging at 150°C for two hours, a relatively large fraction of the defects were faulted loops rather than stacking fault tetrahedra.

#### B. Electropolishing

A very fast method of obtaining specimens was found. The electrolyte used was 50% HCl, 25% ethyl alcohol, and 25% glycerine. The cathode was a stainless steel foil. By electropolishing at a current density of about 3 amp/cm<sup>2</sup> at room temperature, electron microscope specimens could be obtained from a typical foil in about 10 minutes.

#### C. The Microscope

The microscope used was a Siemens Elmikroscop I. Annealing experiments were done with a Valdre double tile hot stage which could be heated

up to 360°C. Using the device the resolution was not very good making quantitative experiments difficult. This was due to the use of a modified objective lens necessary to fit the larger specimen holder.

The orientation of the specimen surface was usually close to [100]; in this case the reflection  $\vec{g}: \langle 002 \rangle$  was used giving small interfringe separation for stacking faults so that the images of the defects were not too distorted. This orientation is a convenient one for distinguishing between stacking fault triangles and tetrahedra. The orientation [111] and  $\vec{g}: \langle 220 \rangle$  was also used in Figs. 12-14.

The magnification was 20,000 on the plates except in a few cases like Fig. 12 where it was 80,000.

### III RESULTS

#### A. Faulted Loops in Gold

Faulted loops were observed having 3, 4, 5 or 6 sides always along  $\langle 110 \rangle$  directions, their sizes varying from  $200\text{\AA}$  to  $4,000\text{\AA}$ .

##### 1. Triangular Loops

Jossang and Hirth<sup>15</sup> calculated the energy of a truncated tetrahedron taking into account all the interaction energies between nonparallel dislocations, but assuming no interaction with the surfaces. They found:

$$\frac{E}{\mu b^3} = \frac{1}{12\pi(1-\nu)} \left( \frac{L}{b} \right) \left[ 2(2-x)\log\left(\frac{\alpha L}{b}\right) + F(x) + \nu G(x) \right] \\ + \sqrt{3} \frac{\gamma}{\mu b} \left( \frac{L}{b} \right)^2 \left[ 1 - 3/4 (1-x)^2 \right]$$

where  $\alpha$  is the parameter taking into account the effect of the core energy.  $F(x)$  and  $G(x)$  are two functions which they tabulated,  $x$  being the parameter describing the truncation of the tetrahedron:

$$x = 2h/\sqrt{3} L$$

i.e.  $x = 1$  if the tetrahedron is complete and  $x = 0$  if the tetrahedron is a triangular fault surrounded by an undissociated  $\frac{1}{3} \langle 111 \rangle$  dislocation.  $L$  is the length of a side of the basal triangle (see Fig. 6).  $\mu$  is the shear modulus,  $\nu$  the Poisson ratio,  $\gamma$  the stacking fault energy, and  $b$  the Burgers vector.

Energy of the defect is plotted as a function of the value of  $x$  in Fig. 7 for  $L = 1000\text{\AA}$ .

Therefore the undissociated triangle should be less stable than one in which the three  $\frac{1}{3} \langle 111 \rangle$  dislocation segments are split into a stair rod and a Shockley partial which glides a short distance into

its glide plane to form a ribbon of stacking fault. Along the three sides of the triangle there should be narrow ribbons of stacking fault in the three other (111) planes. Letting  $h$  be the width of this ribbon at equilibrium and  $x_m$  the corresponding value of the parameter, we next consider the values of  $x_m$  as a function of  $L$ .

Let  $H(x) = F(x) + \nu G(x)$ . The value of  $x_m$  is the smallest positive root of  $dE/dx = 0$ .

$$\frac{1}{\mu b^3} \frac{dE}{dx} = \frac{1}{12\pi(1-\nu)} \frac{L}{b} \left[ -2 \log \alpha \frac{L}{b} + H'(x) \right] + \frac{3\sqrt{3}}{2} \frac{\gamma}{\mu b} \left( \frac{L}{b} \right)^2 (1-x).$$

Hence  $x_m$  is given by

$$H'(x) = 2 \log \alpha \frac{L}{b} + 18\pi \sqrt{3} (1-\nu) \frac{\gamma}{\mu b} \frac{L}{b} (x-1)$$

$$H'(x) = A x + B$$

$$A = 18\pi \sqrt{3} (1-\nu) \frac{\gamma}{\mu b} \frac{L}{b}$$

$$B = 2 \log \alpha \frac{L}{b} - 18\pi \sqrt{3} (1-\nu) \frac{\gamma}{\mu b} \frac{L}{b}$$

In Figs. 8 and 9 and Table I the variation of  $H(x)$  and  $H'(x)$  are shown for different values of  $x$ . The intersection of  $x = H'(x)$  and  $y = Ax + B$  gives the value of  $x_m$  for each value of the parameter  $L$ . (See Fig. 10.)

The values of the coefficient  $A$  and  $B$  as functions of  $L$  are given in Table II. The results are given in Table II and Fig. 11. In all of these calculations the values taken for the different parameters are:

$$\alpha = 4$$

$$b = 3A$$

$$\nu = 0.42$$

$$\frac{\gamma}{\mu b} = 6.2 \times 10^{-3}$$

The results show that the width of the ribbons should always be small, of the order of magnitude of the limit of resolution of the microscope, and it can be observed only in special conditions. This is the case in an  $[111]$  orientation with  $G = [2\bar{2}0]$ . The  $(111)$  and  $(11\bar{1})$  stacking fault planes are not in contrast while two planes of the small ribbons  $(1\bar{1}1)$  and  $(\bar{1}11)$  are in contrast. These two ribbons are clearly visible in Figs. 12-14 in spite of their small size.

In fig. 12 one can see clearly that the defect at the lower right is a tetrahedron whereas that at the upper right is a dissociated triangle. The magnification is 80,000 on the plate and 1,600,000 on the print.

In Fig. 14 the same area is shown with the three different values of  $G$  possible in this orientation close to  $[111]$ . One stacking fault ribbon is out of contrast for each reflection.

## 2. Faulted Loops With More Than Three Sides

For these defects it was also observed that the  $\frac{1}{3}\langle 111 \rangle$  dislocation segments were dissociated.

a. Four-sided loops. There exist two shapes as shown in Figs. 5b and 5c. The shape of 5b could be the result of the intersection of a triangle with the surface. This is very probable since the thickness of the foil is often of the order of magnitude of the size of the loop. Proof of this can be seen in Figs. 15a-15f, detail A. There is no stacking fault ribbon on one side of the loop which is therefore the intersection of the loop and the surface.

The shape of Fig. 5c is probably the one sketched on Fig. 16a. The two black lines bordering two sides of the loop are the ribbons of

stacking fault. This picture was taken with  $G = 220$  which explains why the other ribbons were invisible. This shape cannot be simply the result of intersection of a triangle with the surface.

b. Five-sided loops and hexagons. Stacking fault ribbons were found also in this case. Figure 17c with  $G = [11\bar{3}]$  (in this case three stacking fault planes are visible) is a good example. One possible shape of this defect has been sketched in Fig. 16b.

Diffraction contrast due to ribbons can also be seen in Fig. 18. Only a few hexagons were found but they also seem to be extended. This conclusion is also confirmed by annealing experiments.

#### B. Shrinkage of Defects

Annealing experiments were made in the hot stage. They were mostly qualitative observations because the temperature was not known within better than  $5^{\circ}\text{C}$ , and the resolution did not allow measurement of the size of the loops with accuracy.

Parallel experiments made using the normal stage, hence with better resolution, complete this work. The results are shown in Figs. 19-22. The results of these observations are:

i) At a temperature over  $340^{\circ}\text{C}$  the faulted loops shrunk at a fast enough rate to be observed. If the specimen was held at this temperature they eventually disappeared.

ii) At  $370^{\circ}\text{C}$  the annealing was very fast. All planar defects are annealed out in less than 5 minutes.

iii) During the annealing, the sides of the loops always remain parallel to  $\langle 110 \rangle$ . No faulted circular loop was ever found, even with very slow annealing such as  $310^{\circ}\text{C}$  for 48 hours.

iv) As has been observed by other investigators, tetrahedra did not shrink at an appreciable rate in this temperature range.

#### IV. DISCUSSION

Annealing of quenched gold has been studied previously by electrical resistivity measurements.<sup>4,11</sup> These authors found no step in the resistivity curves which would correspond to the disappearance of faulted loops at 350°C, only a slight recovery at 400°C which was explained by another phenomenon.<sup>6,16</sup>

Their failure to detect a recovery stage at 350°C can be explained by the thermal treatment they applied to their specimens. After quenching they aged their specimens at 25°C. As has been pointed out previously faulted loops do not appear if aging is carried out below 100°C. It is of interest to consider the possible reasons for this observation.

##### A. Formation of Faulted Loops

###### 1. Triangles

Three main possibilities exist to explain the formation of faulted triangles.

i) Interaction between a tetrahedron which is larger than critical size and a dislocation.<sup>8,17</sup> Depending on the Burgers vector of the cutting dislocation either a stacking fault triangle or a dislocation segment is the result.

ii) Nucleation of a Shockley on one face or at a corner of the tetrahedron.<sup>18</sup> This mechanism requires a large activation energy as shown for instance on Fig. 7 in the case of a tetrahedron of 1000Å. However it occurs during observation as shown on Fig. 23 due to high stresses created in the specimen by the electron beam.

iii) Nucleation and growth as a planar defect. The black spot defects that are observed might grow and at some stage collapse to

form a  $\frac{1}{3}$   $\langle 111 \rangle$  dislocation loop.<sup>19,20</sup>

It is possible that after the quench, there are nuclei for both tetrahedra and faulted loops (or black spot defects). If the aging temperature is over 120°C both tetrahedra and faulted loops can grow by absorption of vacancies. If the temperature is under 80°C only tetrahedra can grow.

## 2. Faulted Loops Other Than Triangles

The faulted loops such as Fig. 5b can also be explained as a result of interaction between a triangle and a dislocation as emphasized by Washburn and Saada.<sup>21</sup> Of course it can also be a triangle intersecting the surface. However, other loops, five-sided loops for instance, are not likely to be formed by such intersections. It would require several intersections with the same loop. The most likely explanation seems to be that planar vacancy defects are somehow nucleated and grow in various shapes.

### B. Shrinkage of Loops

Two experimental facts must be explained: The temperature at which shrinkage occurs and the fact that defects keep the same shape while shrinking.

#### 1. The Temperature

It is of interest to consider why planar vacancy defects in gold are much less stable than tetrahedra.

a. The annealing of tetrahedra. It has been explained by three different mechanisms.

i) Transformation of a tetrahedron to a triangle, by nucleation of a Shockley,<sup>8,17</sup> then shrinkage of the triangle by emission of vacancies. This mechanism requires a very high activation energy and is

therefore improbable.<sup>15</sup>

ii) Interstitial atoms eat up the defect. This has been observed in irradiated gold, but it is doubtful that it can happen in quenched metals where the interstitial concentration is very small.<sup>23,24</sup>

iii) Ledge mechanism. This mechanism has received much discussion.<sup>4,6,8,15,25,27</sup> Although no direct evidence has yet been obtained in the case of stacking fault in gold, the same mechanism, responsible for growth of precipitates in Ag-Al alloys, was observed in hot stage experiments by Hren and Thomas.<sup>29</sup> For shrinkage the mechanism is essentially the emission of a vacancy at a stair rod dislocation, most probably at a corner of the tetrahedron.<sup>4,6</sup> Nucleation and then migration of "I ledges" (see Fig. 24a) can explain the shrinkage of tetrahedra. The activation energy of the process (4.7 eV after Meshii<sup>11</sup>) implies a very low value of the energy per atomic length of the stair rod dipole, (about 1/20 eV), which does not seem unreasonable. From resistivity measurements it is observed that the annealing temperature for tetrahedra is about 650°C.

c. The annealing of faulted loops. The faulted loops in gold are extended. Therefore, they may also have to shrink by a ledge mechanism. This process requires the nucleation of I ledges which in case of tetrahedra needed a high activation energy. The fact that faulted loops anneal at a lower temperature may indicate that nucleation of I ledges on sides like DE, EF, DF (Fig. 24c) which are Shockley dislocations instead of stair rod, require a smaller activation energy. It is probable that the nucleation would be easier at the corners D, E, F, which are different from corners like A, B, C.

## 2. The Shape of Defects During Annealing

The triangular shape is a rather high energy configuration. The

loops should become hexagons or circular loops as soon as the temperature is high enough to allow vacancies to move. This did not happen and is explained by the fact that triangles are extended; the formation of a new side would require a rather high activation energy.

The result is slightly different in the case of loops with more than three sides. Corner A (see Fig. 16b) can be removed more easily than the corners of a triangle. It was sometimes observed that a five-sided loop became a four-sided loop during the shrinkage.

All defects remained prismatic during shrinkage, with their sides along  $\langle 110 \rangle$  directions. Since they are extended, the shrinkage may also be explained in terms of a ledge mechanism, involving an activation energy close to that required for shrinkage of triangles, probably a little lower since the nucleation of a ledge at a  $120^\circ$  corner, where the two ribbons are not on the same side of the loop, should be easier than for a  $60^\circ$  corner.

## V. CONCLUSIONS

1. Both stacking fault tetrahedra and stacking fault loops of various shape are formed from excess vacancies when quenched gold is aged at 150°C.
2. Edges of all defects were always parallel to a [110] direction.
3. From the energy of a truncated tetrahedron<sup>15</sup> it was shown that stacking fault triangles in gold should be extended. Experimental evidence of this was obtained, using special conditions of diffraction in observing the defects with an electron microscope.
4. Faulted loops with more than three sides were also found to be extended.
5. Annealing experiments showed that planar defects shrink at a lower temperature than tetrahedra (about 350°C) and that their sides remain parallel to  $\langle 110 \rangle$  during shrinkage.
6. The observations are consistent with a ledge mechanism for shrinkage.

ACKNOWLEDGMENTS

The author expresses his deep gratitude to Professor Jack Washburn for his continued interest and encouragement and to Professor Gareth Thomas for his valuable suggestions. He also wishes to thank Dr. P. C. J. Gallagher for assistance with the tilting hot stage.

This work was supported under the auspices of the United States Atomic Energy Commission through the Inorganic Materials Research Division of the Lawrence Radiation Laboratory.

TABLE I

x	H(x)	H'(x)
0.001	14.434	
0.005	11.238	-799.0
0.01	9.882	-271.2
0.02	8.500	-138.2
0.03	7.770	-73.0
0.04	7.227	-54.3
0.05	6.810	-41.7
0.06	6.471	-33.9
0.07	6.186	-28.5
0.08	5.940	-24.6
0.09	5.722	-21.8
0.10	5.529	-19.3
0.20	4.255	-9.20
0.30	3.505	-6.35
0.40	2.986	-4.55
0.50	2.623	-3.10
0.60	2.387	-1.90
0.70	2.269	-0.70
0.80	2.270	+0.45
0.90	2.414	+2.10
1.00	2.860	+7.75

TABLE II

L (Å)	A	B	$x_m$	h(Å)
200	27	-15.9	0.2	34.64
230	--	-----	0.15	29.6
500	67.5	-54	0.045	19.4
1000	135	-120	0.022	19.0
2000	270	-255	0.011	19.0
3000	405	-383	0.008	20.7

REFERENCES

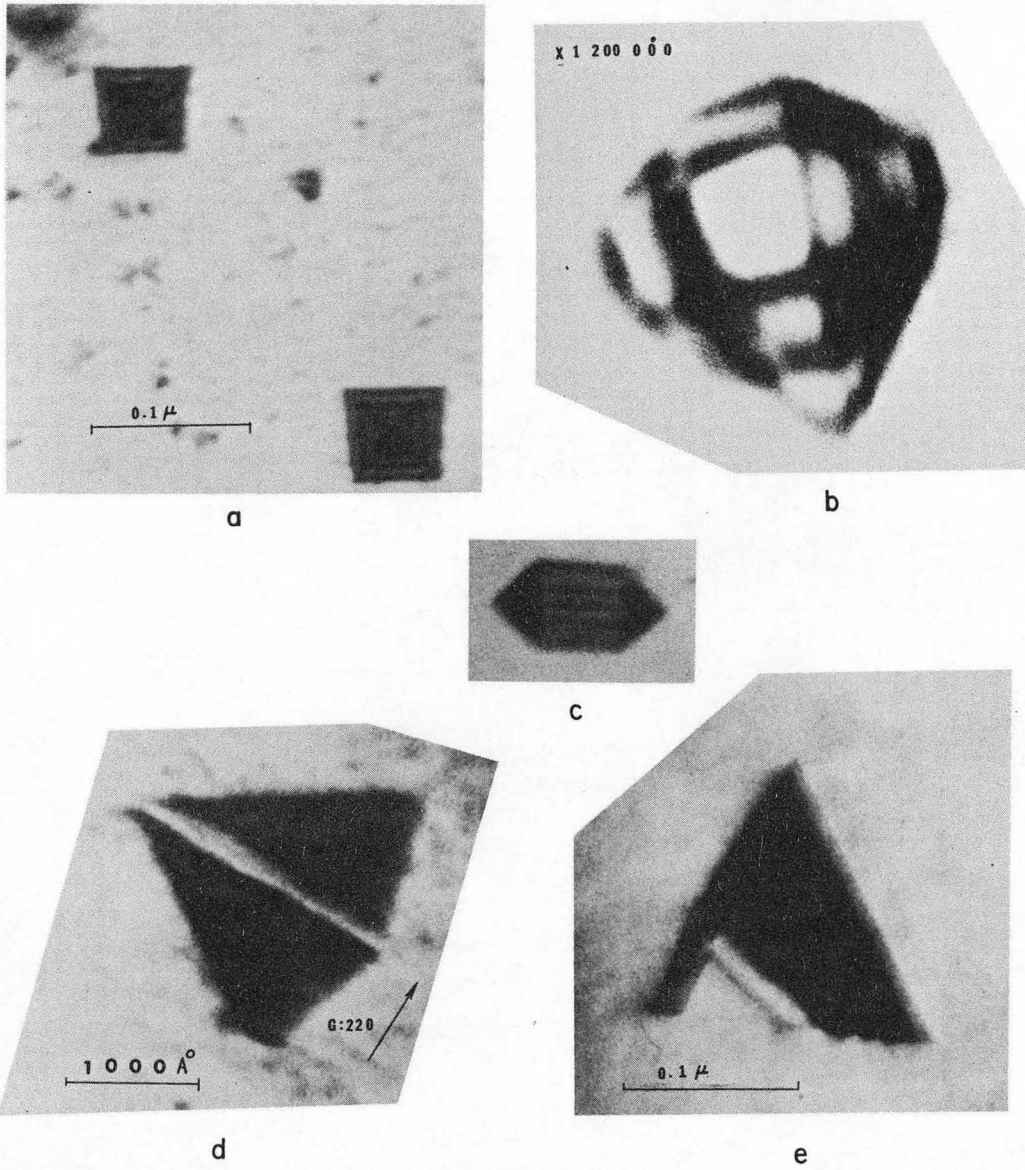
1. Silcox and Hirsh, *Phil. Mag.* 4, 72 (1959).
2. Hirsh, *Phil. Mag.* 7, 67 (1962).
3. Loretto, Clarebrough and Segall, *Phil. Mag.* 11, 459 (1965).
4. De Jong and Koehler, *Phys. Rev.* 129, 1 (1963).
5. Kimura, Kuhlmann-Wilsdorf, and Maddin, *Appl. Phys. Letters*, 3, 4 (1963).
6. Cotterill and Doyama, *Appl. Phys. Letters*, 4, 25 (1964).
7. Kuhlmann-Wilsdorf, Kimura and Maddin, *J. Appl. Phys.* 35, 2557 (1964).
8. Kuhlmann-Wilsdorf, *Acta Met.* 13, 257 (1965).
9. Czjzek, Seeger, and Mader, Max Planck Report, 1962 (Stuttgart).
10. Saada, *Acta Met.* 10, 551 (1962).
11. Meshii, Lattice Defects in FCC Metals, (Academic Press, New York, 1963) p. 387.
12. Cotterill, Lattice Defects in FCC Metals, (Academic Press, New York, 1963) p. 97.
13. Cotterill, *J. Phys. Soc. Japan*, 18, Suppl. III. 48 (1963).
14. Ytterhus, and Balluffi, *Phil. Mag.*, 11, 707 (1965).
15. Jossang and Hirth, *Phil. Mag.*, 13, 657 (1966).
16. Cotterill, *Phil. Mag.*, 6, 1351 (1961).
17. Kimura and Maddin, Lattice Defects in FCC Metals, (Academic Press, New York, 1963) p. 366.
18. Meshii and Kaufmann, *Phil. Mag.*, 5, 939 (1960).
19. Kuhlmann-Wilsdorf, and Wilsdorf, *J. Appl. Phys.*, 31, 516 (1960).
20. Thomas and Washburn, *Rev. Mod. Phys.* 35, 4 (1963).
21. Saada and Washburn, UCRL Report 10427.
22. Tartour (to be published).
23. Venables and Balluffi, *Bull. Am. Phys. Soc. Ser.*, 11, 295 (1964).

24. Hirsh, Proc. 5th. Conf. of Electron Microscopy, Vol. I, F3 (1963).
25. Kuhlmann-Wilsdorf and Maddin, Appl. Phys. Letters, 3, 3 (1963).
26. Silcox, Ph.D. Dissertation, University of Cambridge, 1961.
27. Segall, Clarebrough, and Loretto, Phil. Mag., 14, 53 (1966).
28. Bell, Maher and Thomas, Lattice Defects in Quenched Metals (Academic Press, New York, 1963) p. 739.
29. Hren and Thomas, Trans. AIME, 227 (1963).

FIGURE CAPTIONS

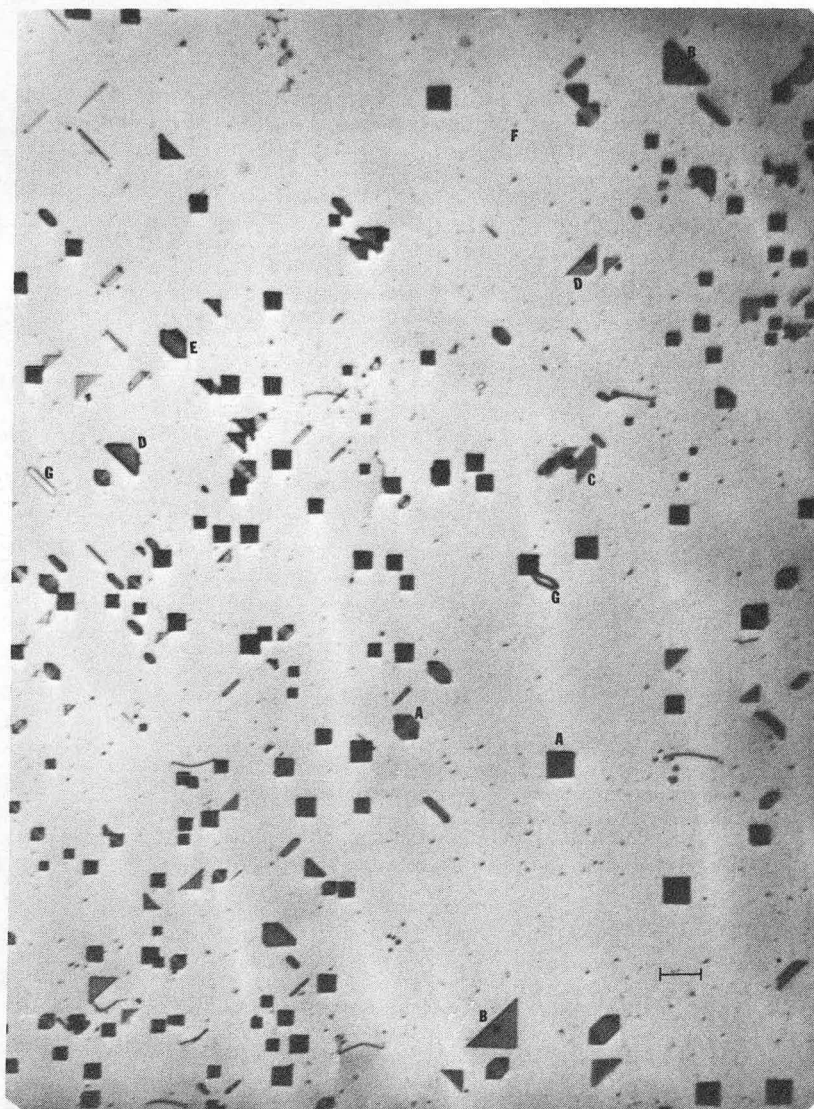
- Fig. 1 Different aspects of stacking fault tetrahedra. a) orientation  $[100] G = [020]$  b) orientation close to  $[100] G = [220]$ .
- Fig. 2 Defects in gold after a quench from  $1050^{\circ}\text{C}$  in brine at  $20^{\circ}\text{C}$ , the preaging time is about 20 sec.
- Fig. 3 Defects in gold after same quench as above but the preaging time is two minutes.
- Fig. 4 Quenching curves: a) water at  $20^{\circ}\text{C}$ , b) brine at  $20^{\circ}\text{C}$ , c) water at  $0^{\circ}\text{C}$ , d) brine at  $-20^{\circ}\text{C}$ .
- Fig. 5 Faulted loops.
- Fig. 6 The real shape of triangular defects.
- Fig. 7 Plot  $E(x)$ , the energy of a truncated tetrahedron of side  $L = 1000\text{\AA}$  as a function of the truncation.
- Fig. 8  $H(x)$  (cf. Table I).
- Fig. 9  $H'(x)$  (cf. Table II).
- Fig. 10 Graphic determination of the root of  $H'(x) = Ax + B$ .
- Fig. 11 Plot  $h(L)$  giving the width of the stacking fault ribbon as a function of the size  $L$  of the triangle.
- Fig. 12 Stacking fault ribbon and tetrahedron seen at the magnification 1,600,000.
- Fig. 13 Triangles and tetrahedra in a  $[111]$  orientation with  $G = [220]$ .
- Fig. 14 The same area seen under 3 different  $G$  of the type  $\langle 220 \rangle$ .
- Fig. 15 The same area seen under six different values of  $G$ .
- Fig. 16 Sketch of 4- and 5-sided loops.
- Fig. 17 The same area under 3 different  $G$ .
- Fig. 18 A five-sided loop in 2 different  $G$ .
- Fig. 19 Hot stage experiment, each after 10 minutes at  $340^{\circ}\text{C}$ .

- Fig. 20 Hot stage: a) before, b) after 5' at 350°C, c) after 22' at 350°C.
- Fig. 21 Hot stage: a) before, b) 5' at 350°C.
- Fig. 22 Hot stage: a) before, b) 11' at 350°C.
- Fig. 23 Transformation tetrahedron triangle under the beam in the microscope. The two pictures are taken at ten minutes intervals.
- Fig. 24 Ledges on a tetrahedron. a) I Ledges, b) V Ledges.



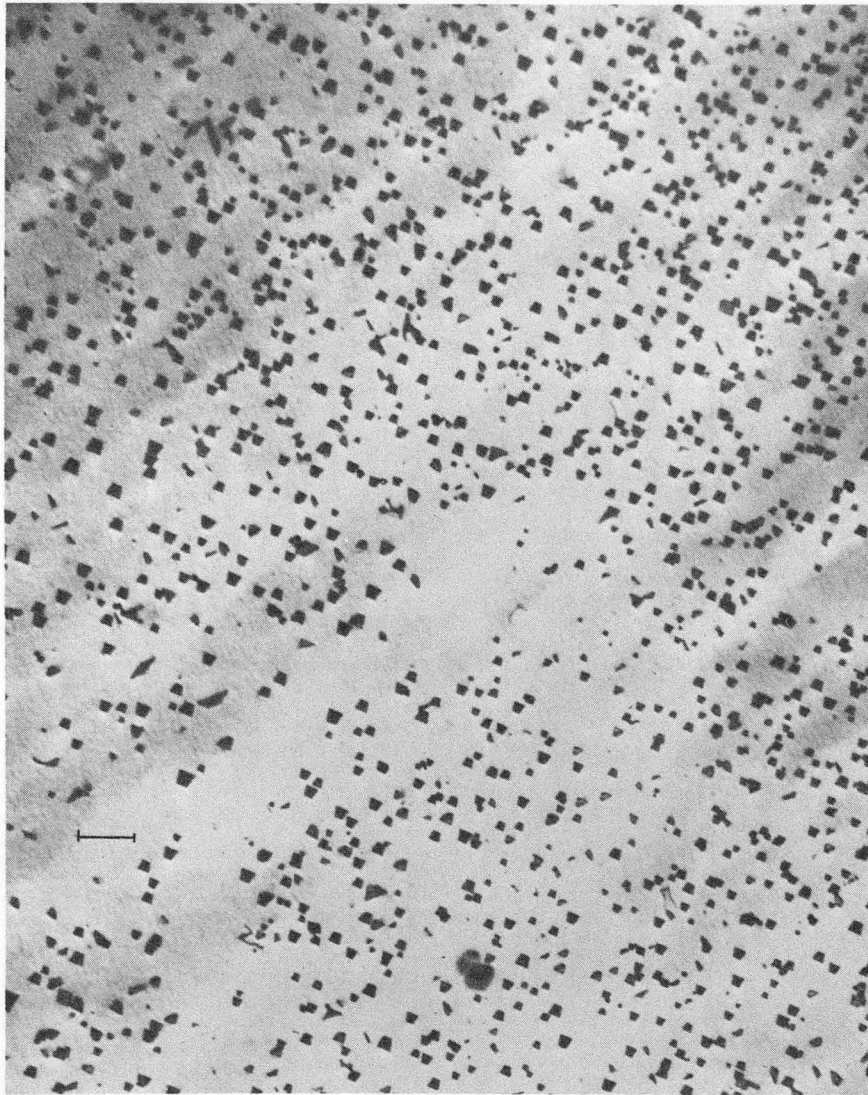
ZN-5860

Fig. 1



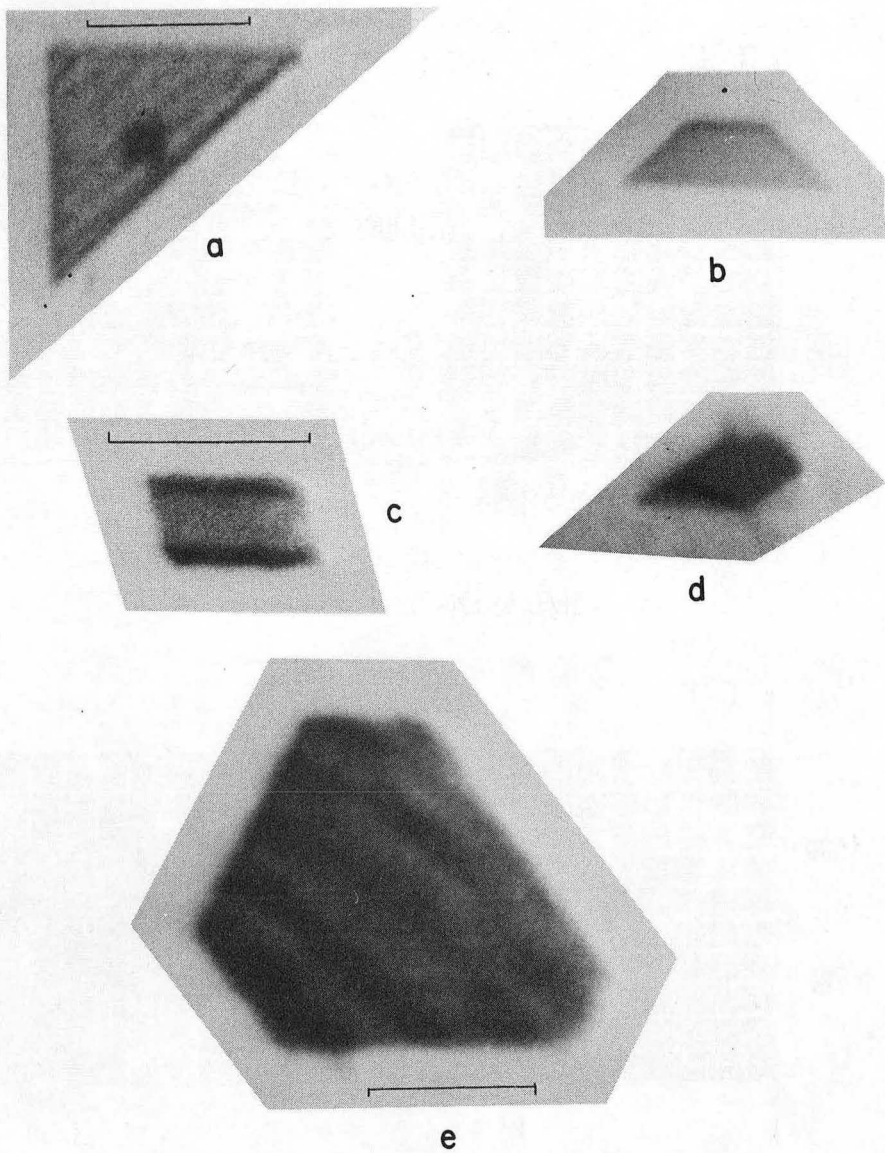
ZN-5892

Fig. 2



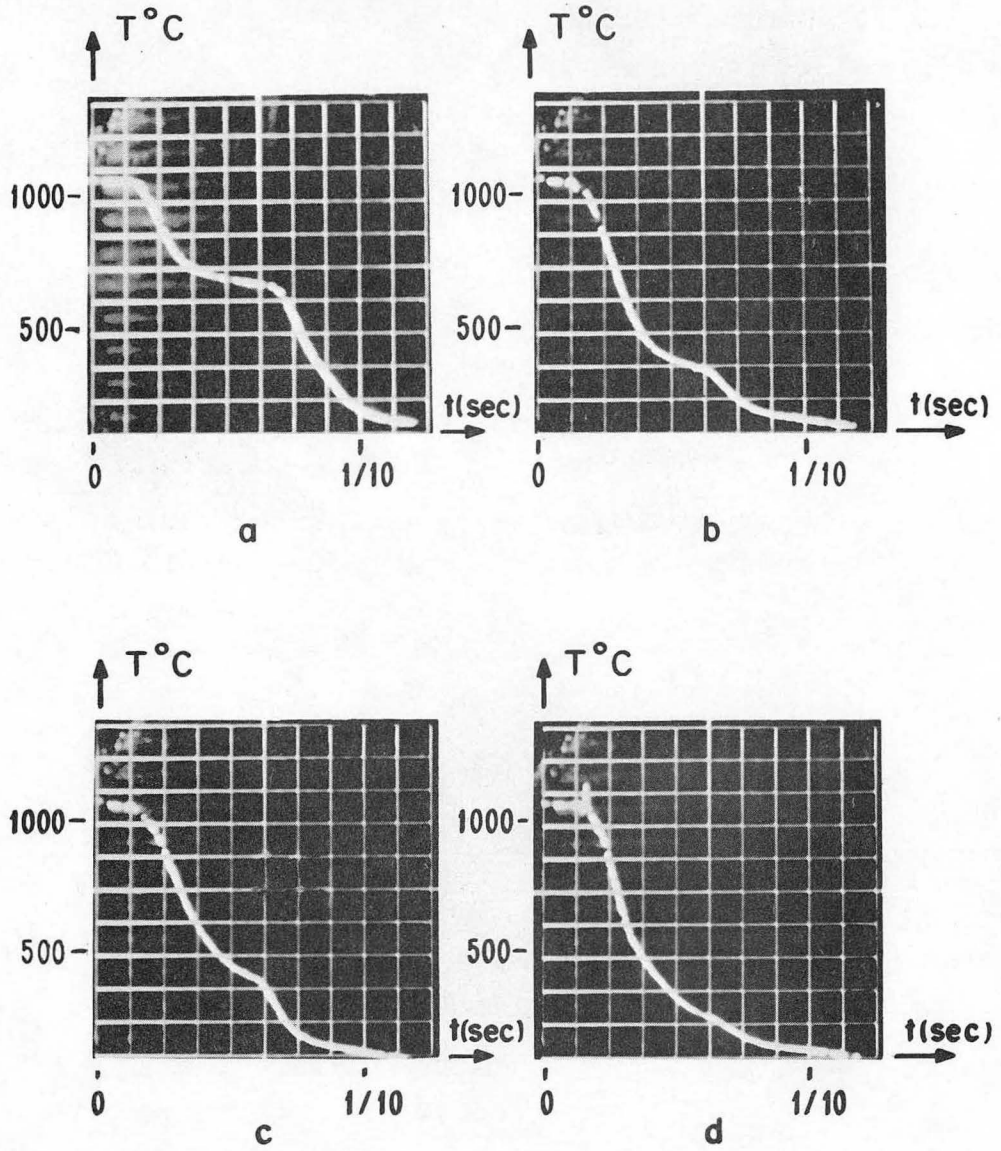
ZN-5891

Fig. 3



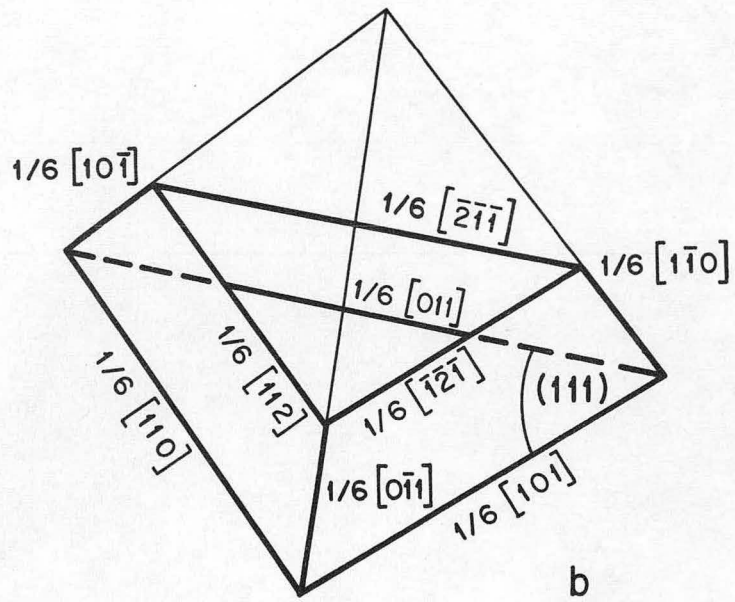
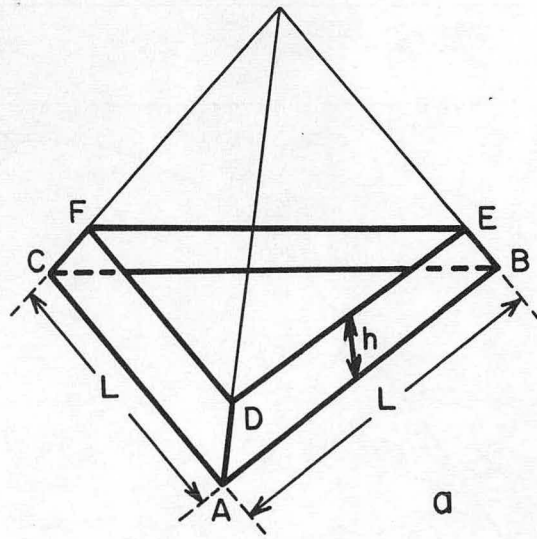
ZN-5861

Fig. 4



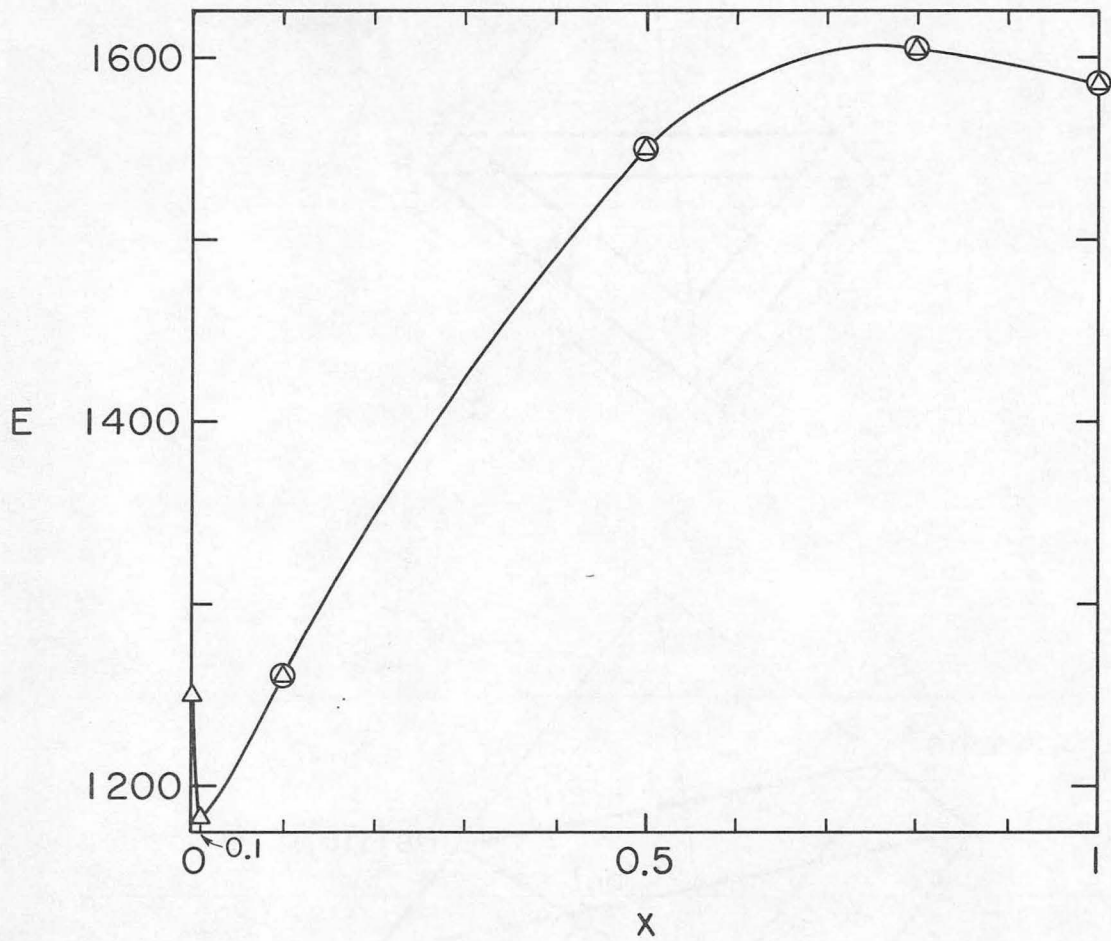
ZN-5862

Fig. 5



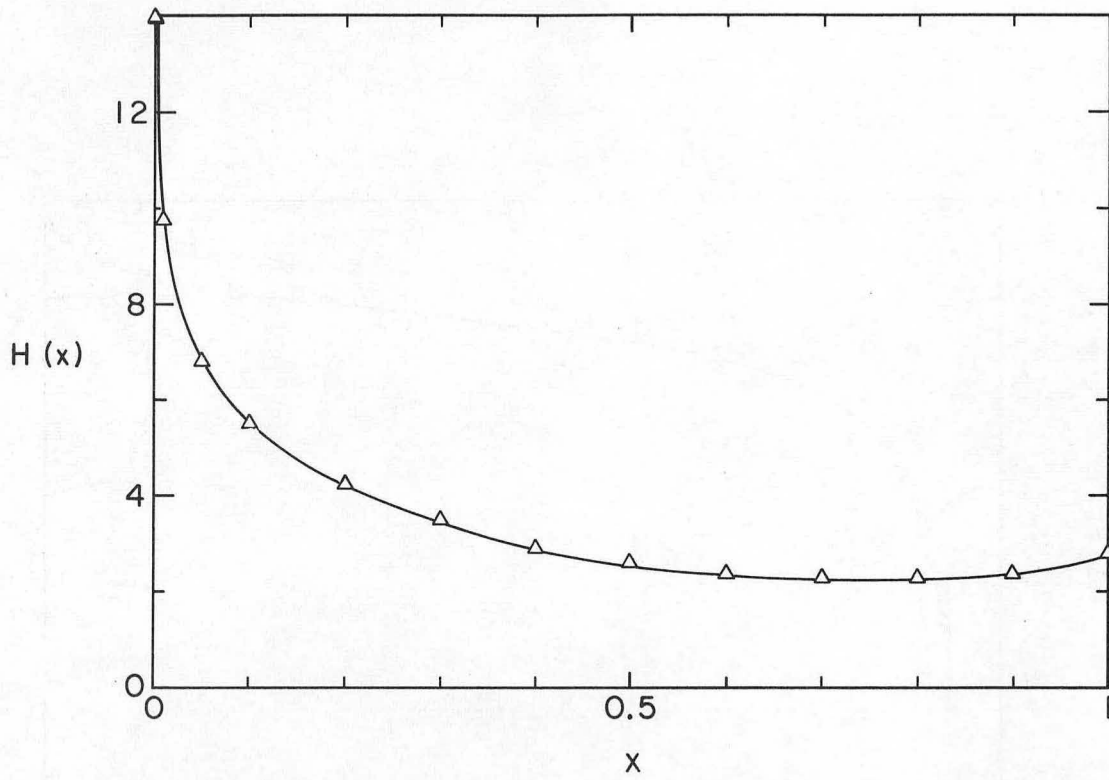
MUB-12272

Fig. 6



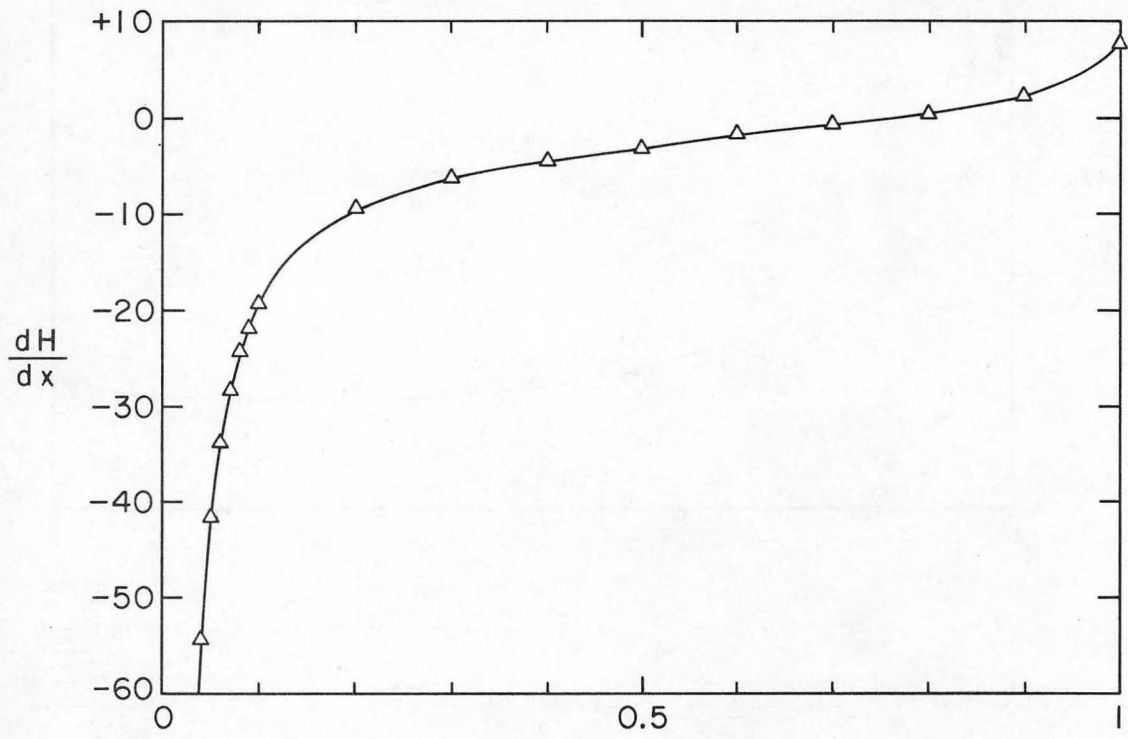
MUB-12273

Fig. 7



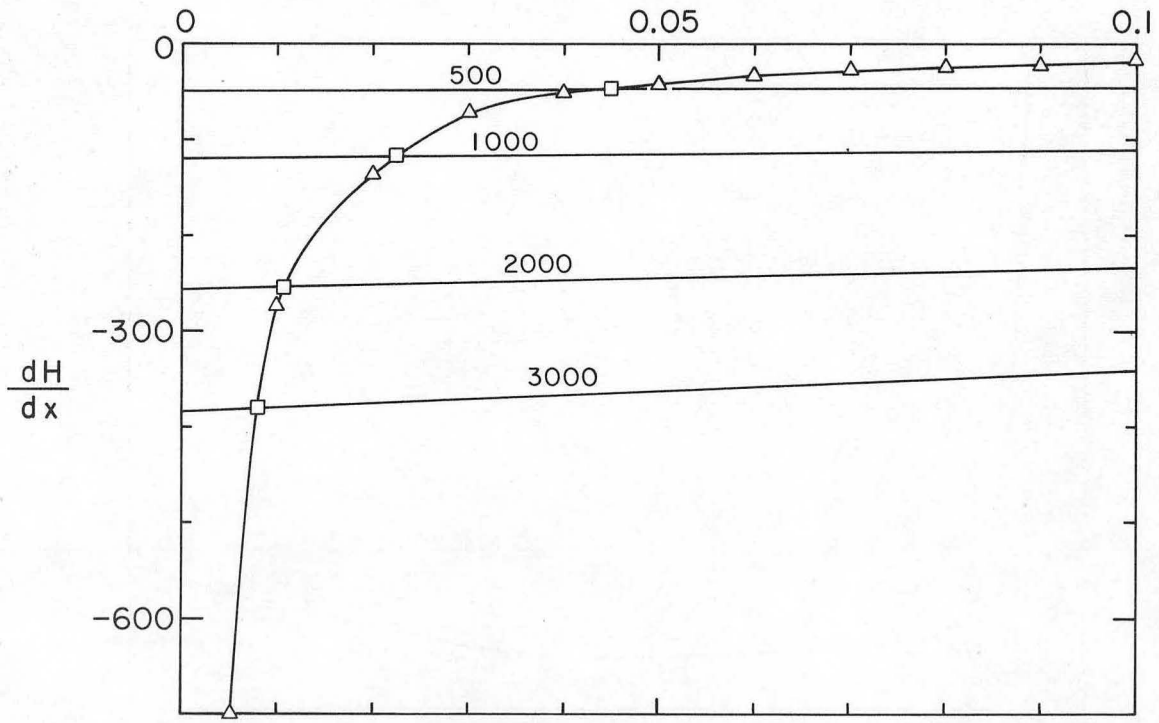
MUB-12274

Fig. 8



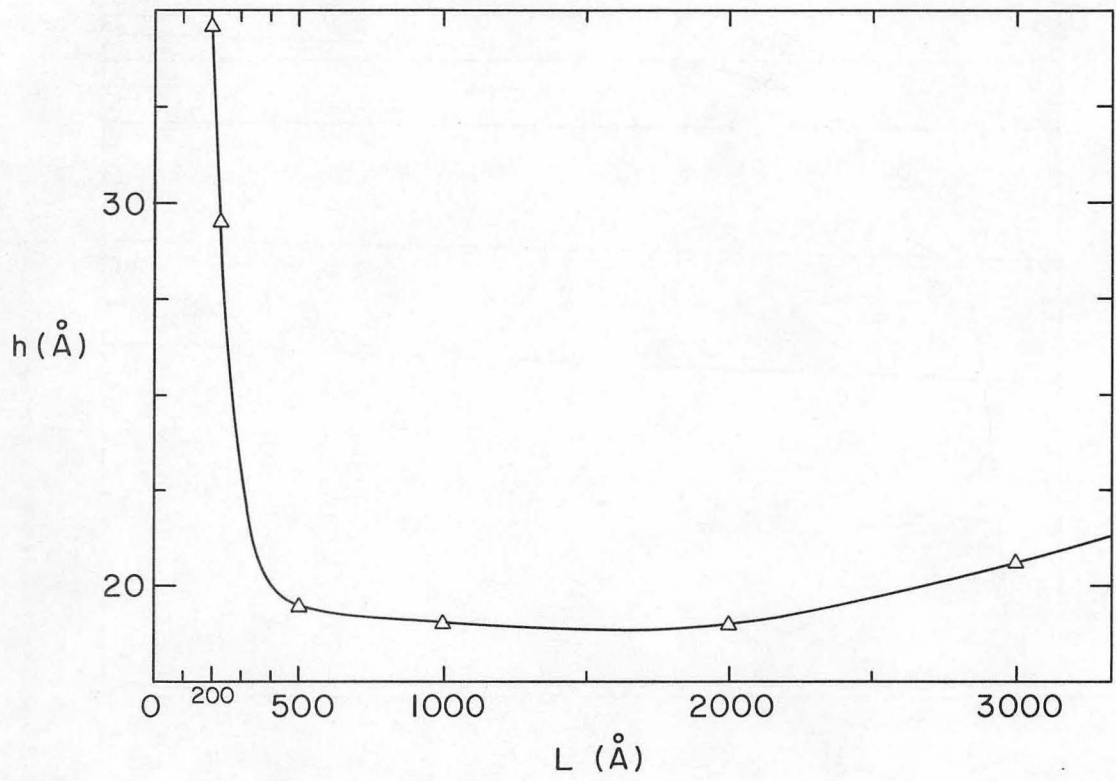
MUB-12275

Fig. 9



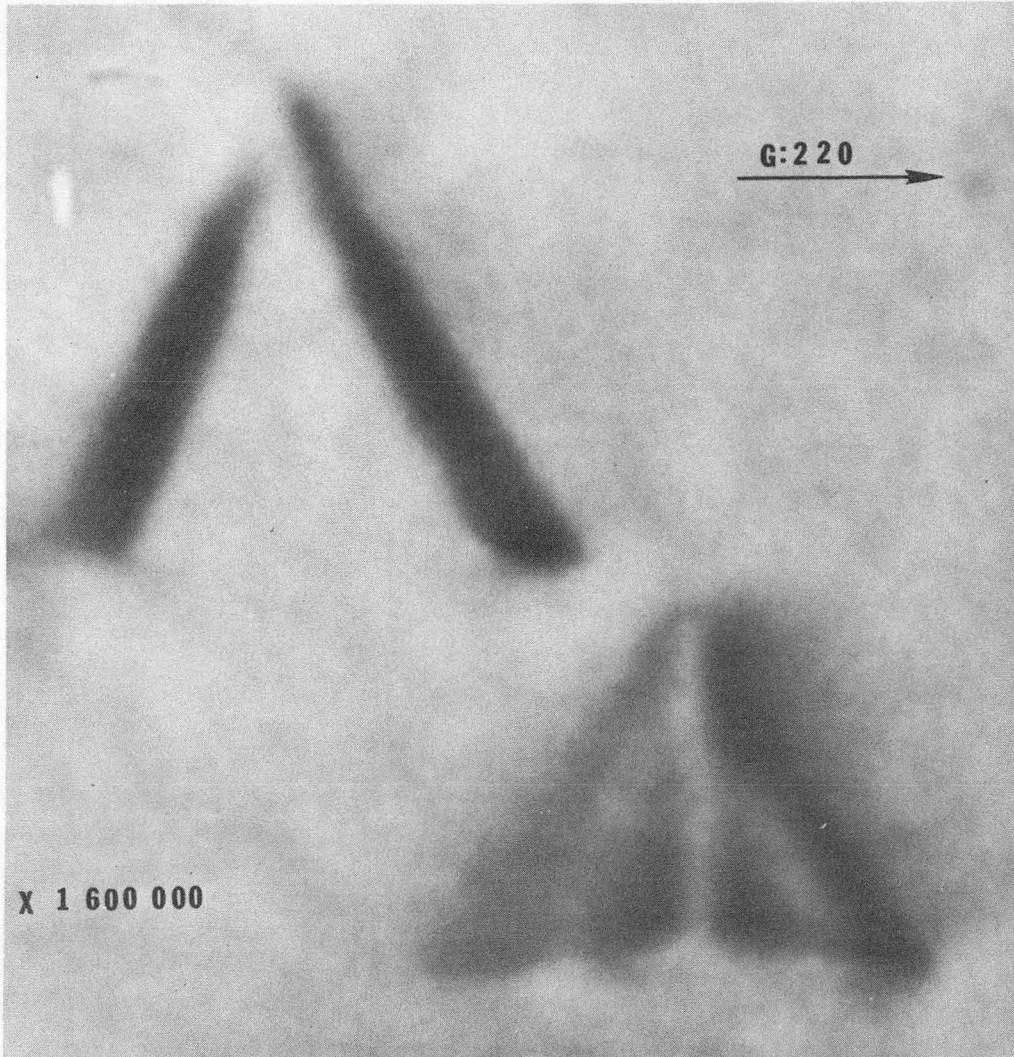
MUB-12276

Fig. 10



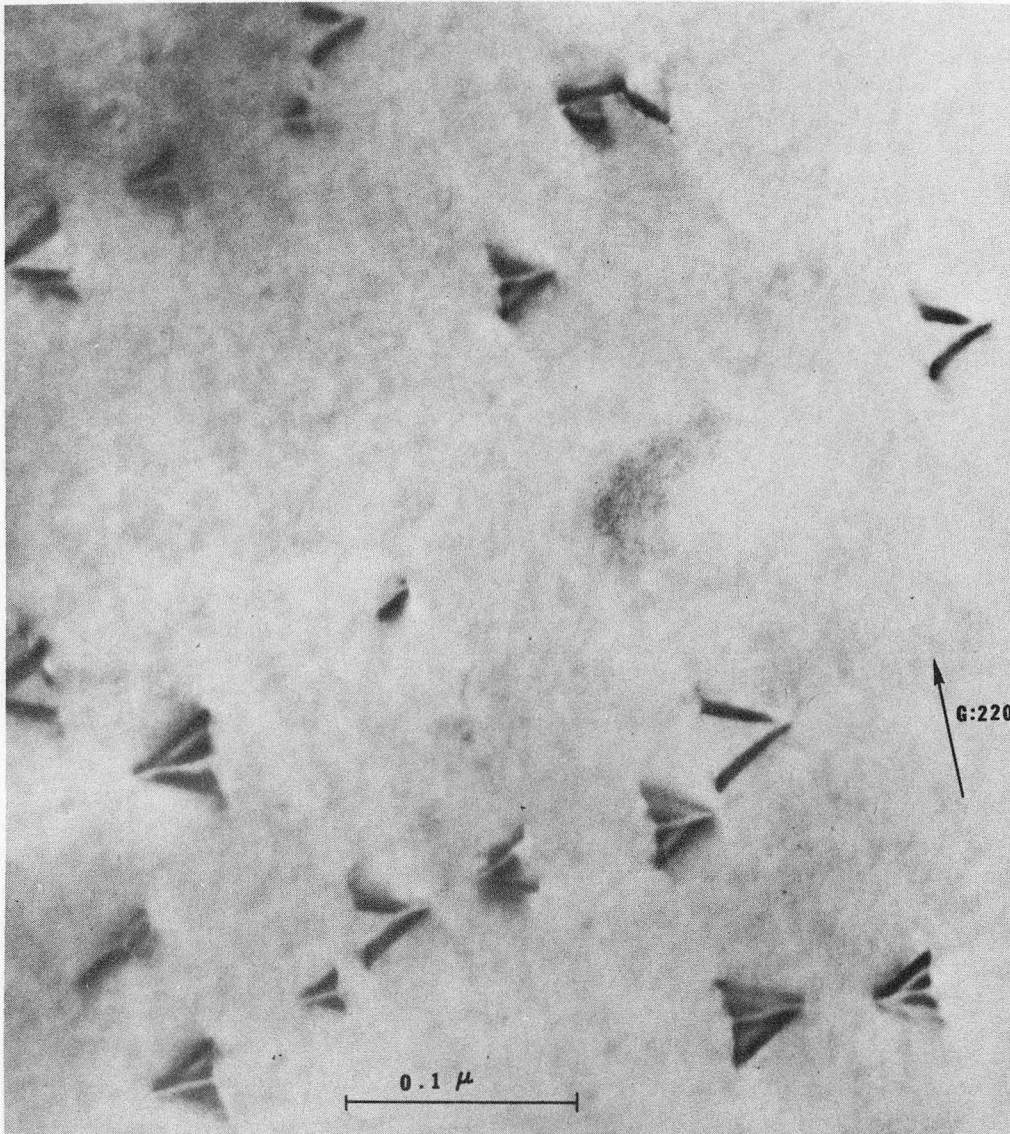
MUB-12277

Fig. 11



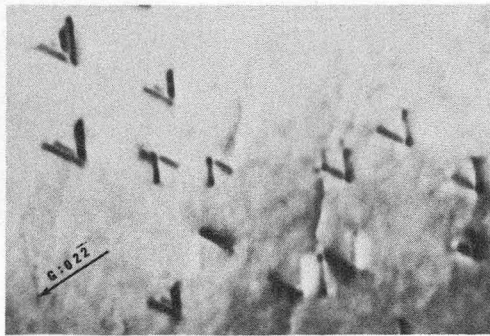
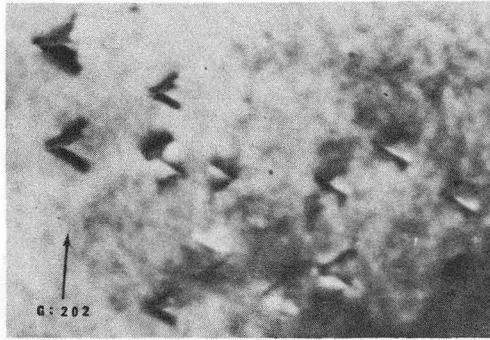
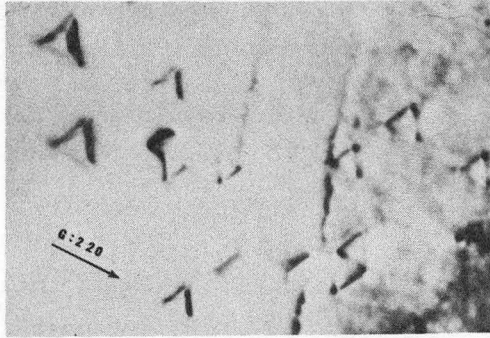
ZN-5890

Fig. 12



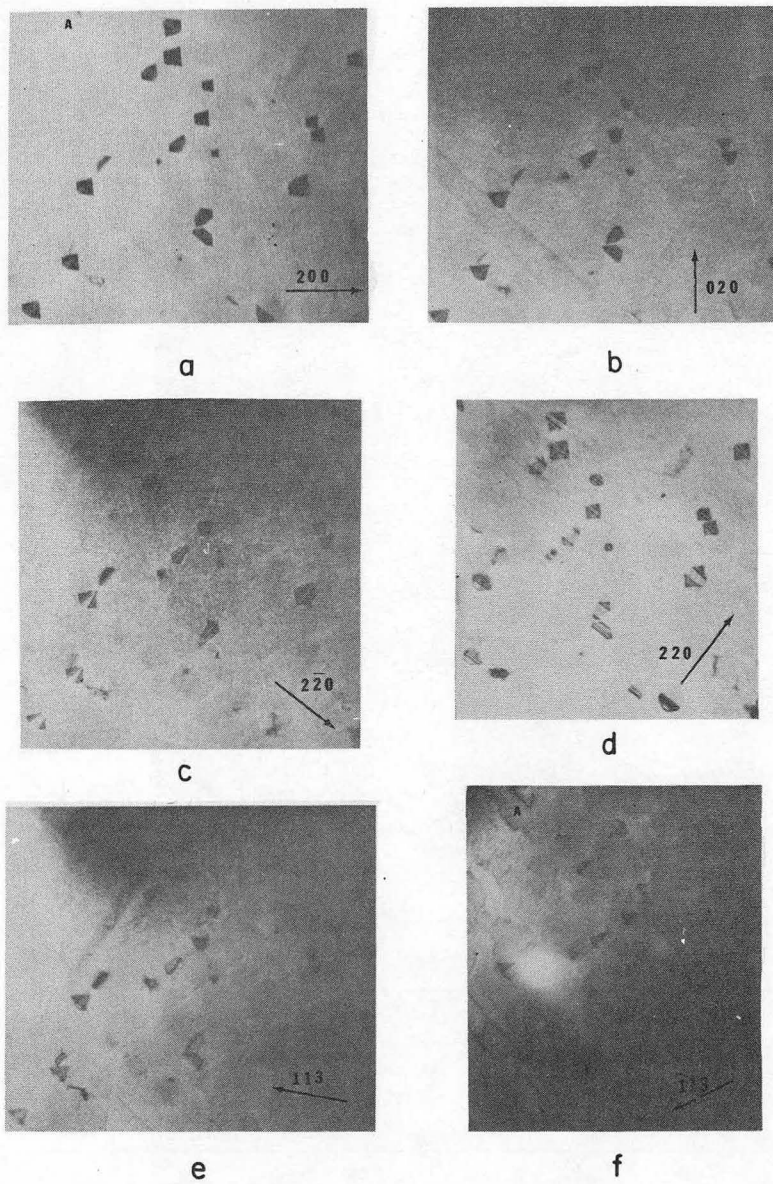
ZN-5889

Fig. 13



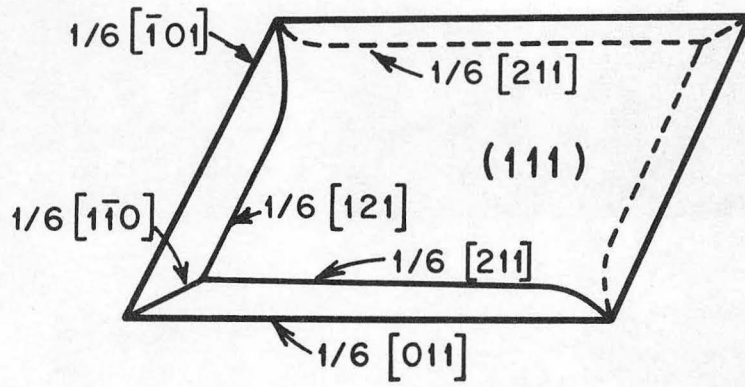
ZN-5888

Fig. 14

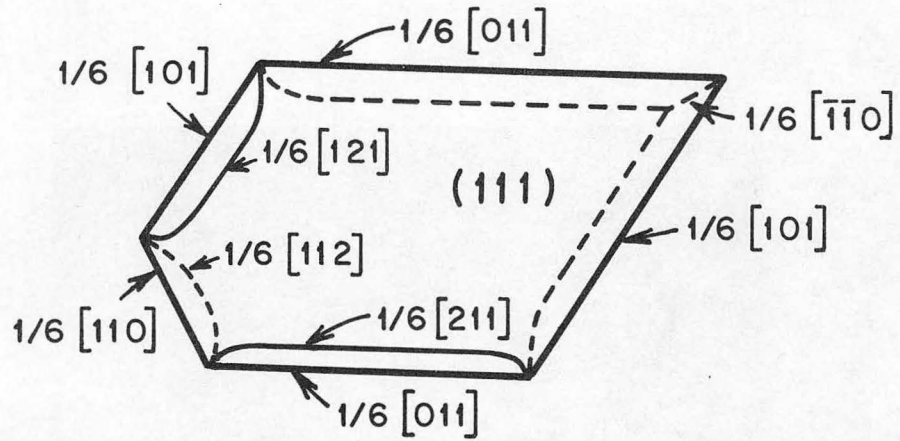


ZN-5869

Fig. 15



a



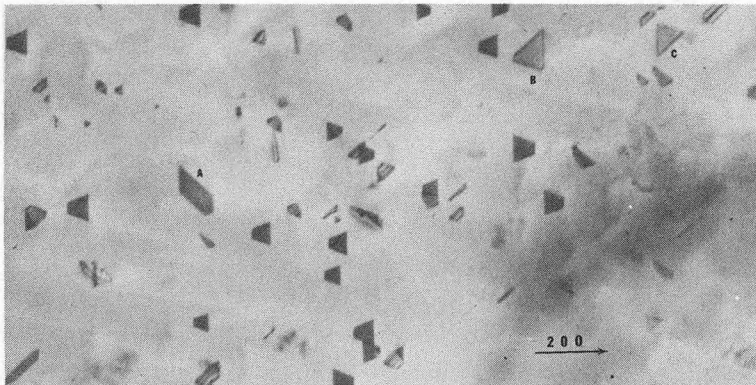
b

MUB-12278

Fig. 16



D



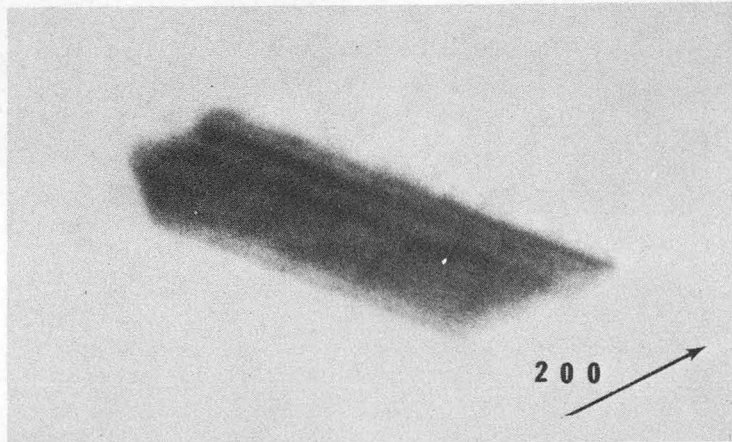
b



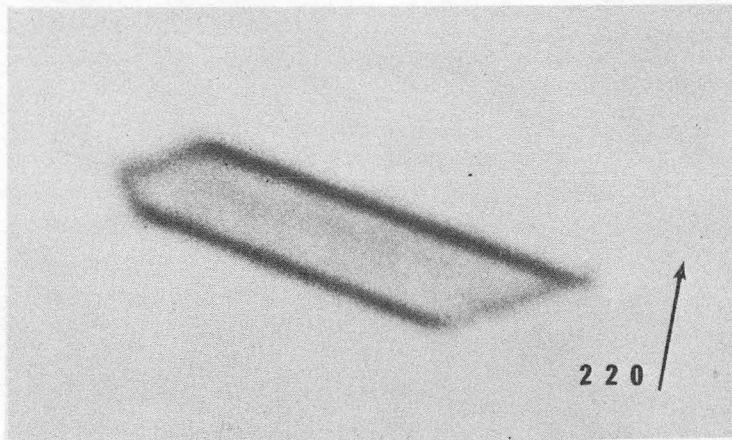
c

ZN-5866

Fig. 17



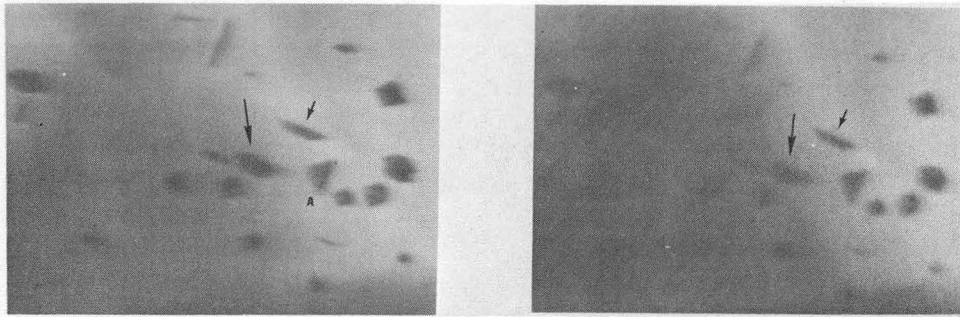
a



b

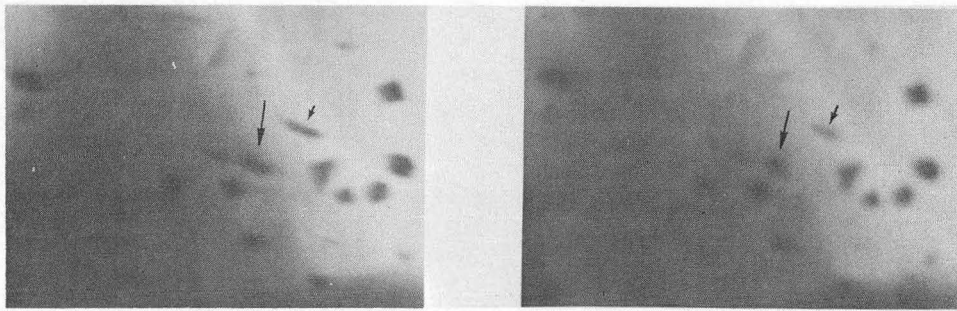
ZN-5865

Fig. 18



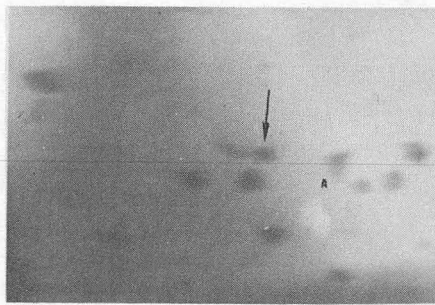
a

b



c

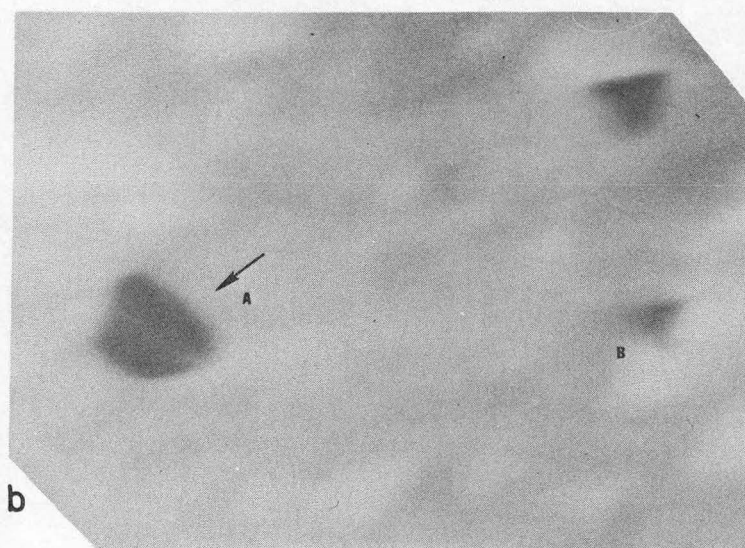
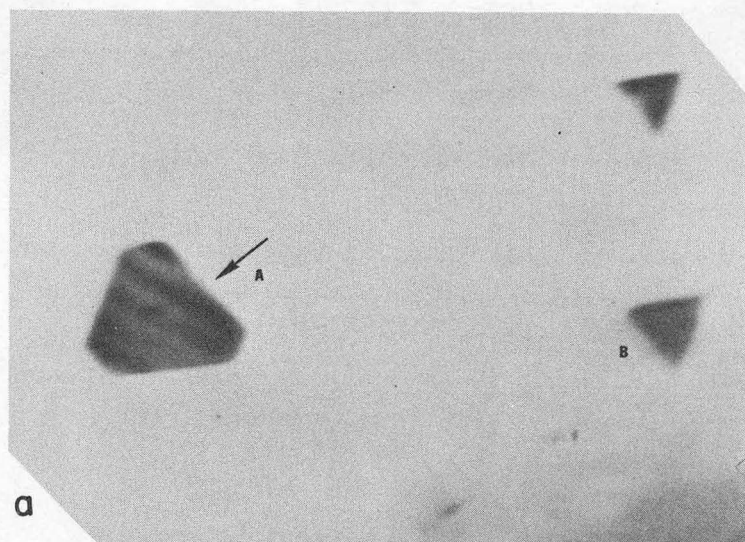
d



e

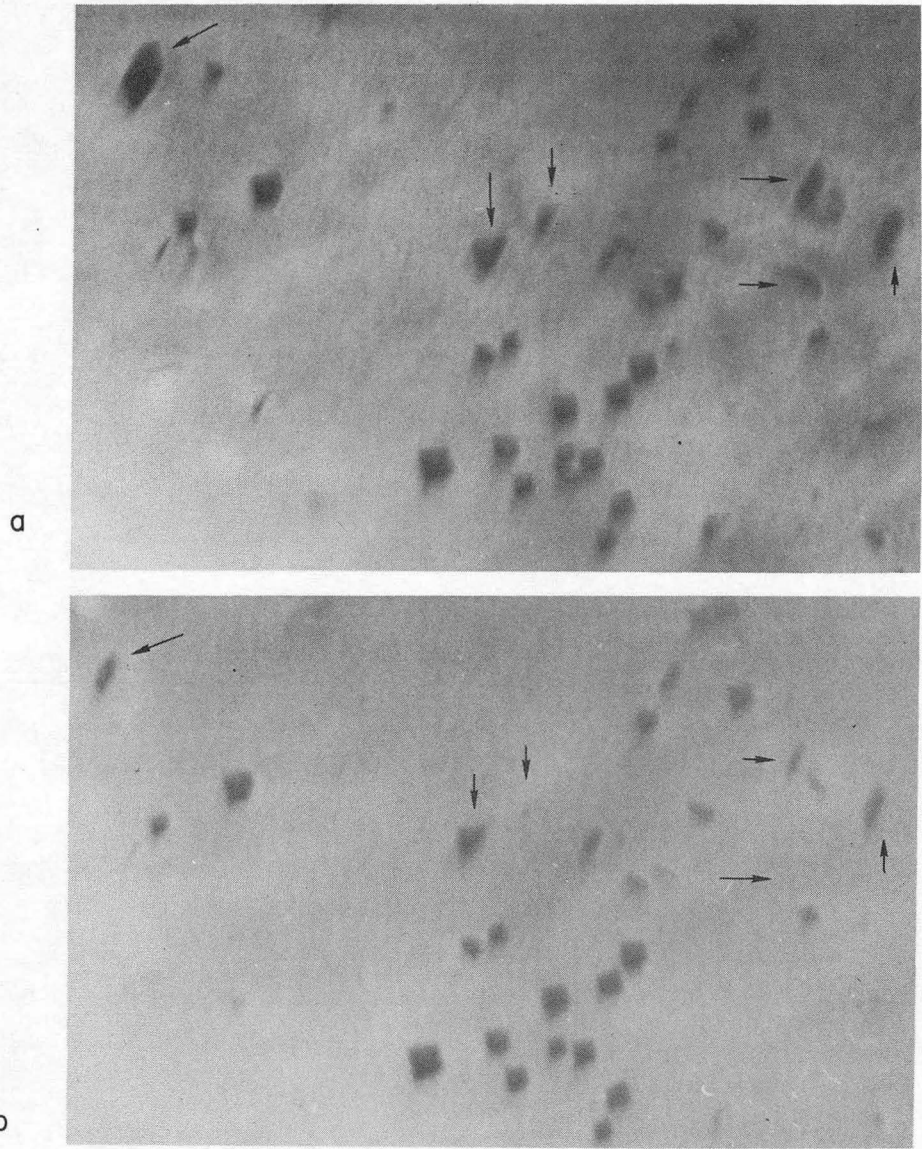
ZN-5867

Fig. 19



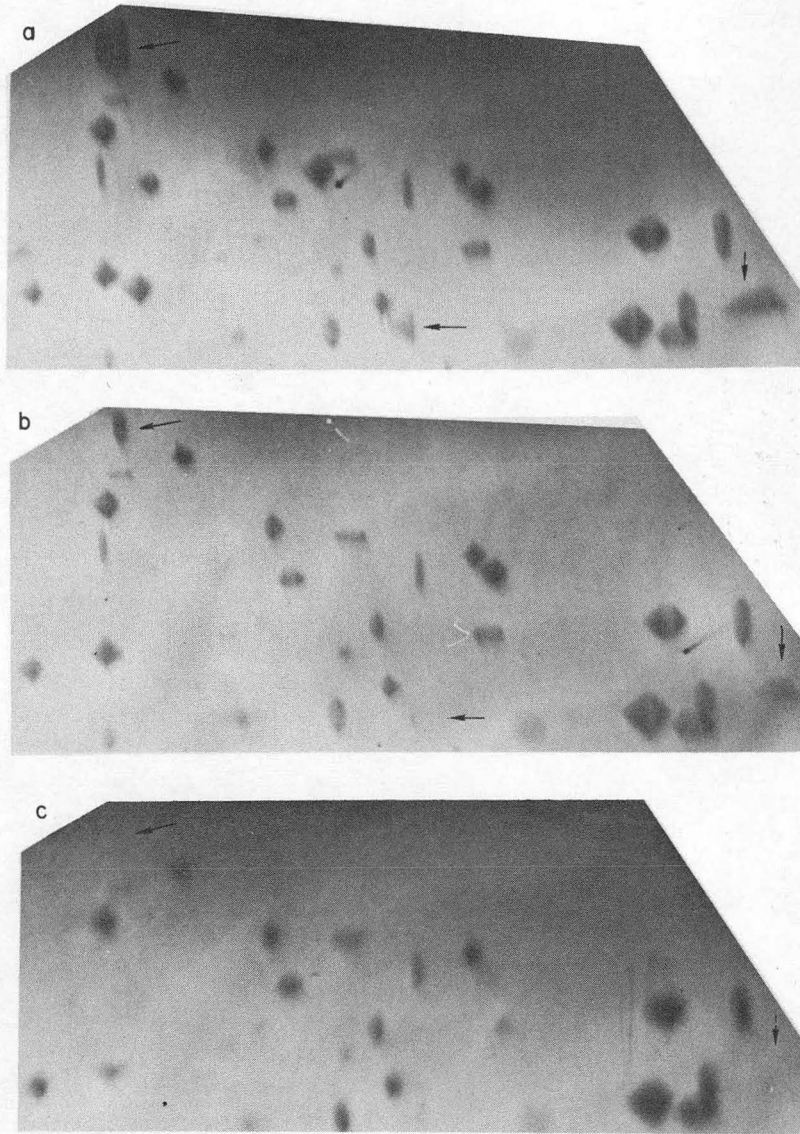
ZN-5863

Fig. 20



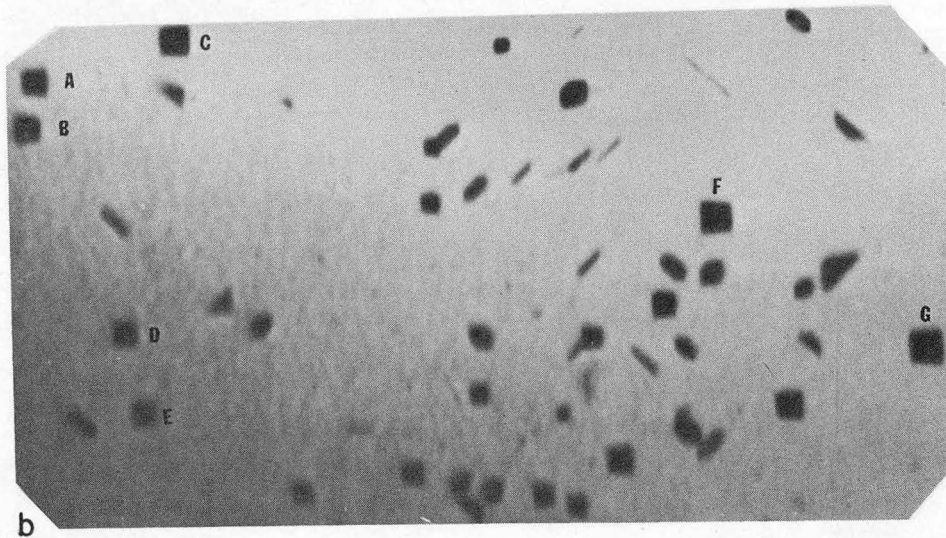
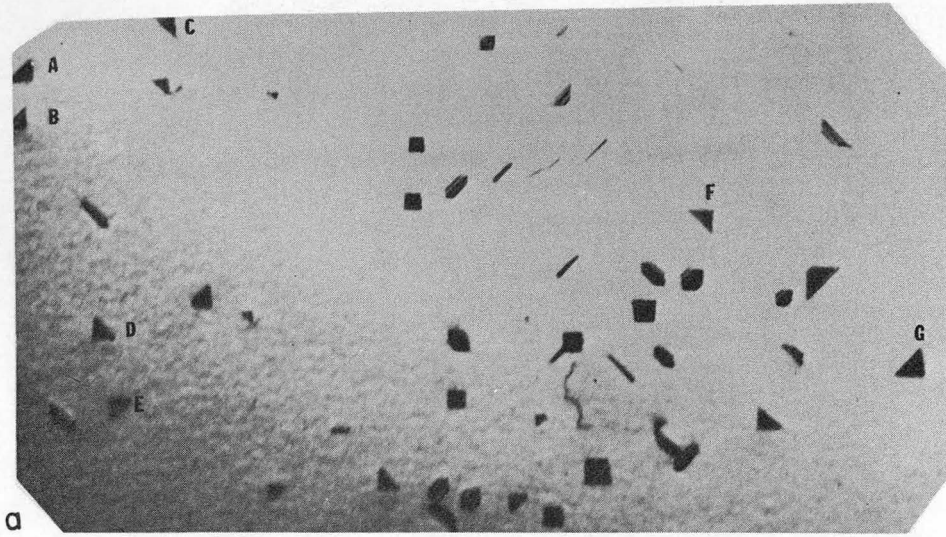
ZN-5868

Fig. 21



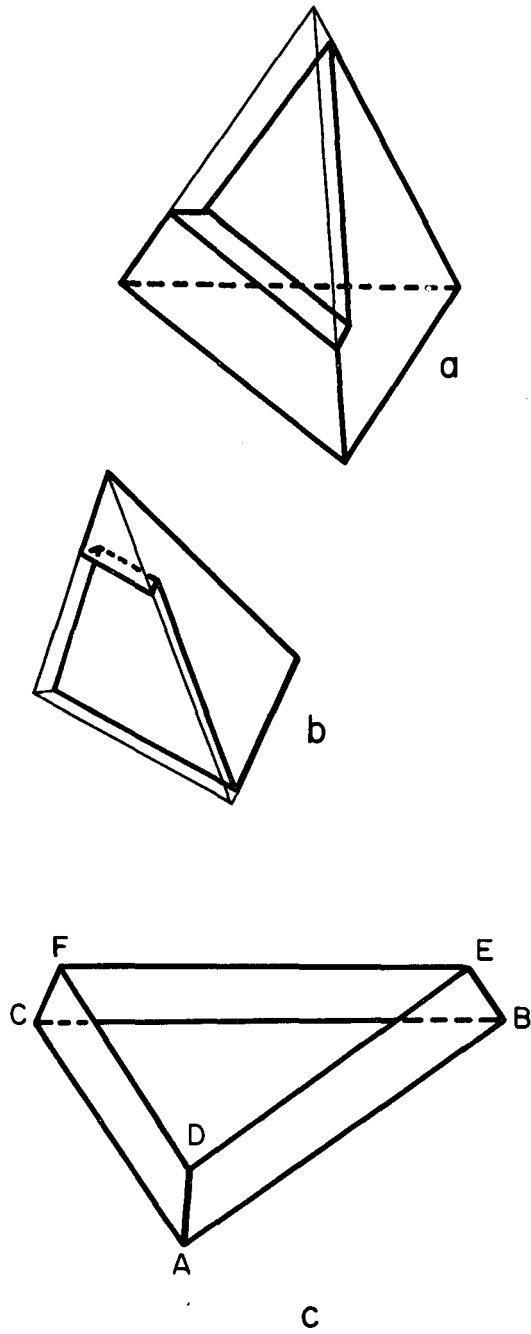
ZN-5870

Fig. 22



ZN-5864

Fig. 23



MUB 12279

Fig. 24

This report was prepared as an account of Government sponsored work. Neither the United States, nor the Commission, nor any person acting on behalf of the Commission:

- A. Makes any warranty or representation, expressed or implied, with respect to the accuracy, completeness, or usefulness of the information contained in this report, or that the use of any information, apparatus, method, or process disclosed in this report may not infringe privately owned rights; or
- B. Assumes any liabilities with respect to the use of, or for damages resulting from the use of any information, apparatus, method, or process disclosed in this report.

As used in the above, "person acting on behalf of the Commission" includes any employee or contractor of the Commission, or employee of such contractor, to the extent that such employee or contractor of the Commission, or employee of such contractor prepares, disseminates, or provides access to, any information pursuant to his employment or contract with the Commission, or his employment with such contractor.

